Fabio Remondino
David Stoppa *Editors*

TOF Range-Imaging Cameras

Springer

TOF Range-Imaging Cameras

Fabio Remondino · David Stoppa
Editors

TOF Range-Imaging Cameras

Springer

Editors
Fabio Remondino
3D Optical Metrology
Fondazione Bruno Kessler
Trento
Italy

David Stoppa
Smart Optical Sensors and Interfaces
Fondazione Bruno Kessler
Trento
Italy

ISBN 978-3-642-27522-7 ISBN 978-3-642-27523-4 (eBook)
DOI 10.1007/978-3-642-27523-4
Springer Heidelberg New York Dordrecht London

Library of Congress Control Number: 2013935255

Printed on acid-free paper

Springer is part of Springer Science+Business Media (www.springer.com)

Contents

State-of-the-Art of TOF Range-Imaging Sensors 1
Dario Piatti, Fabio Remondino and David Stoppa

SPAD-Based Sensors 11
Edoardo Charbon, Matt Fishburn, Richard Walker,
Robert K. Henderson and Cristiano Niclass

Electronics-Based 3D Sensors 39
Matteo Perenzoni, Plamen Kostov, Milos Davidovic,
Gerald Zach and Horst Zimmermann

Sensors Based on In-Pixel Photo-Mixing Devices 69
Lucio Pancheri and David Stoppa

Understanding and Ameliorating Mixed Pixels and Multipath Interference in AMCW Lidar 91
John P. Godbaz, Adrian A. Dorrington and Michael J. Cree

3D Cameras: Errors, Calibration and Orientation 117
Nobert Pfeifer, Derek Lichti, Jan Böhm and Wilfried Karel

TOF Cameras for Architectural Surveys 139
Filiberto Chiabrando and Fulvio Rinaudo

Indoor Positioning and Navigation Using Time-Of-Flight Cameras . . . 165
Tobias K. Kohoutek, David Droeschel, Rainer Mautz and Sven Behnke

TOF Cameras and Stereo Systems: Comparison and Data Fusion 177
Carlo Dal Mutto, Pietro Zanuttigh and Guido M. Cortelazzo

TOF Cameras in Ambient Assisted Living Applications 203
Alessandro Leone and Giovanni Diraco

State-of-the-Art of TOF Range-Imaging Sensors

Dario Piatti, Fabio Remondino and David Stoppa

1 Introduction

The 3D information of a surveyed object or scene can be recorded with different types of sensors and measuring techniques. Contactless measuring techniques suitable to estimate the target distance exploit micro-, ultrasonic- or light- waves [1, 2]. However only the latter technique allows achieving good angular resolution performance, in a compact measuring setup, as required for a 3D imaging system [3]. In the common practice, the two ways to acquire an object's geometry are: (i) passive, by using multi-view image data or (ii) active, exploiting optical distance measurement techniques.

The multi-view image acquisition method, coupled with the triangulation measurement principle, is already known and used for decades in the research community [4]. One of the advantages of the image approach with respect to other range measuring devices (such as LiDAR, acoustic or radar sensors) is the reachable high resolution and simultaneous acquisition of the surveyed area without energy emission or moving parts. Still, the major disadvantages are the correspondence problem, the processing time and the need of adequate illumination conditions and textured surfaces in the case of automatic matching procedures.

Active optical measuring techniques using light-waves can be further classified in three main categories, namely: interferometry, triangulation and Time-Of-Flight (TOF) [5–7]. Triangulation techniques normally determines an unknown point

D. Piatti (✉)
Politecnico di Torino, Corso Duca degli Abruzzi 24 10129 Turin, Italy
e-mail: dario.piatti@polito.it

F. Remondino · D. Stoppa
Fondazione Bruno Kessler, Via Sommarive 18 38123 Trento, Italy
e-mail: remondino@fbk.eu

D. Stoppa
e-mail: stoppa@fbk.eu

F. Remondino and D. Stoppa (eds.), *TOF Range-Imaging Cameras*,
DOI: 10.1007/978-3-642-27523-4_1, © Springer-Verlag Berlin Heidelberg 2013

within a triangle by means of a known optical basis and the related side angles pointing to the unknown point. This principle is used by active sensors based on structured illumination as well as by passive digital cameras.

Continuous wave and pulse TOF techniques measure the time of flight or the phase shift of a modulated optical signal. These techniques usually apply incoherent optical signals. Typical examples of TOF are the optical rangefinder of total stations or classical LiDAR instruments (terrestrial or aerial) [8, 9]. In this latter case, actual laser scanners allow to acquire almost one million of points per second, thanks to fast scanning mechanisms. Their measurement range can vary to a great extent according to the instruments, varying between some decimeters up to some kilometers, with an accuracy ranging from less than one millimeter to some tens of centimeters respectively. Nevertheless, the main drawbacks of LiDAR instruments are their high costs and dimensions.

Interferometry methods measure depths by means of the Time-Of-Flight techniques too. In this case, however, the phase of the optical wave itself is used. This requires coherent mixing and correlation of the wave-front reflected from the object with a reference wave-front. Many variants of the optical interferometry principle have been developed, such as multi-wavelength interferometry, holographic interferometry, speckle interferometry and white light interferometry. The high accuracy of the interferometry methods mainly depend on the coherence length of the light source: interferometry is not suitable for ranges greater than few centimeters since the method is based on the evaluation of very short optical wavelength.

In the last few years a new generation of active sensors has been developed, which allows to acquire 3D point clouds without any scanning mechanism and from just one point of view at video frame rates. The working principle is the measurement of the TOF of an emitted signal by the device towards the object to be observed, with the advantage of simultaneously measuring the distance information for each pixel of the camera sensor. Many terms have been used in the literature to indicate such devices, normally called Time-Of-Flight (TOF) cameras, Range IMaging (RIM) cameras, 3D range imagers, range cameras or a combination of these terms. In the following sections and chapters the term TOF cameras will be prevalently employed, which is more related to the working principle of this technology. Such a technology is possible because of the miniaturization of the semiconductor technology and the evolvement of the CCD/CMOS processes that can be implemented independently for each pixel. Thus it is possible to acquire distance measurements for each pixel at high frame rate and with accuracies up to few centimeters. While TOF cameras based on the phase-shift measurement usually have a working range limited to ten/thirty meters, TOF cameras based on the direct TOF measurement can measure distances up to 1500 m. Moreover, TOF cameras are usually characterized by low resolution (no more than a few thousands of tens of pixels), small dimensions, costs that are an order of magnitude lower with respect to LiDAR instruments and a lower power consumption with respect to classical laser scanners. In contrast to multi-view image acquisitions, the depth accuracy is practically independent of textural appearance, but limited to about one centimeter in the best case.

Recently a great alternative to TOF cameras came on the market: it is the line of sensors based on real-time pattern projection and triangulation technique which enable simultaneous acquisition of geometry and texture, at low-cost, high frame rate and with ranges up to 4–5 m. The most well know sensor of this family is the Microsoft Kinect [10, 11]. This book will not touch such devices as they are not based on the TOF measurement principle.

In order to give an overview on the TOF cameras technology, this chapter will provide a quick introduction of the TOF cameras operation principle and a description of their main building blocks. Then, the main technologies available today for the realization of TOF detectors will be described and compared and finally some conclusions and future perspective will be given.

2 Working Principle of TOF Cameras

2.1 TOF Detection System

A typical TOF measuring setup is sketched in Fig. 1, and it consists of several building blocks: (a) a pulsed/modulated light source, typically based on LASER or LED in the infrared part of the spectrum to make the illumination unobtrusive, (b) an optical diffuser to spread the emitted light onto the scene, (c) a collection lens aimed at gathering the light echo back-reflected by the target. An optical band-pass, properly tuned onto the wavelength of the light source, allows improving the background noise rejection. Finally, the core of the measuring system is represented by the solid-state range sensor (d), composed of an array of photo-detectors (pixels) capable of measuring, in a direct on indirect way, the TOF needed by the light pulse to travel from the light source to the target and back to the sensor. The system requires also a suitable sensor interface providing to the sensor the power supply, required biasing voltage/current signals, digital control phases, and reading out from the sensor the data stream, which typically requires further minor processing to obtain the 3D volume data. Finally, the sensor interface is responsible for the communication with the external world (to a PC, or a processing unit).

2.2 TOF Measurement Techniques

In a classical TOF measurement, referred in the following as Direct-TOF (D-TOF), the detector system starts a highly accurate stopwatch synchronously with the emitter light pulse generation. As the light echo from the target is detected, the stopwatch is stopped and the roundtrip time τ_{TOF} is directly stored. The target distance z can be estimated by means of the simple equation:

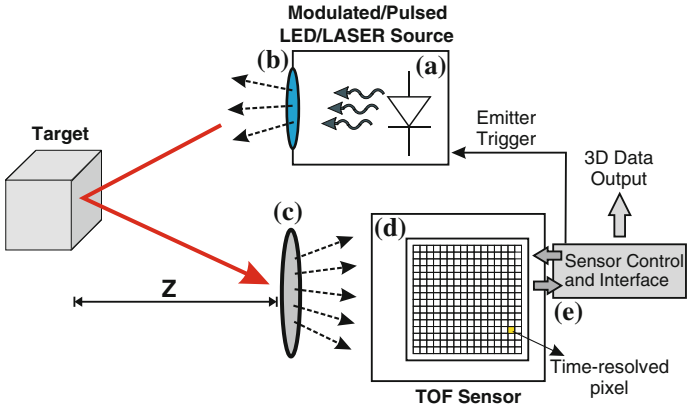

Fig. 1 TOF detection system

$$Z = \frac{c}{2} \cdot \tau_{TOF} \tag{1}$$

where c = 2.9979 × 10^8 m/s represents the speed of the light propagating through the air.

D-TOF is commonly used for single-point range systems, but only recently implemented in scannerless TOF systems, because of the difficulties in implementing at pixel level sub-nanosecond electronic stopwatch. This technique is particularly suited to SPAD-based TOF systems [12–23] and details about its implementation will be described in Chap. 2.

An alternative solution to D-TOF is the so-called Indirect-TOF (I-TOF), where the roundtrip trip time is indirectly extrapolated from a time-gated measurement of the light intensity. In this case, there is no need of precise stopwatch, but of time-gated photons counters or charge integrators, which can be implemented at a pixel level with less efforts and silicon area. I-TOF is the natural solution for electronic- and photo-mixing devices-based TOF cameras.

The operation principle of D-TOF and an example of a four-gates I-TOF are illustrated in Fig. 2 considering both pulsed and modulated light sources, although many other implementations of I-TOF are possible. I-TOF will be extensively described in Chaps. 3 and 4 together with its circuital implementation.

3 Time-Resolved Image Sensor Technologies

Although there are many TOF systems based on laser scanner available on the market for top-class 3D measurement apparatus, there has been in the last decade an emerging interest toward scannerless, all-solid-state, TOF cameras. Many

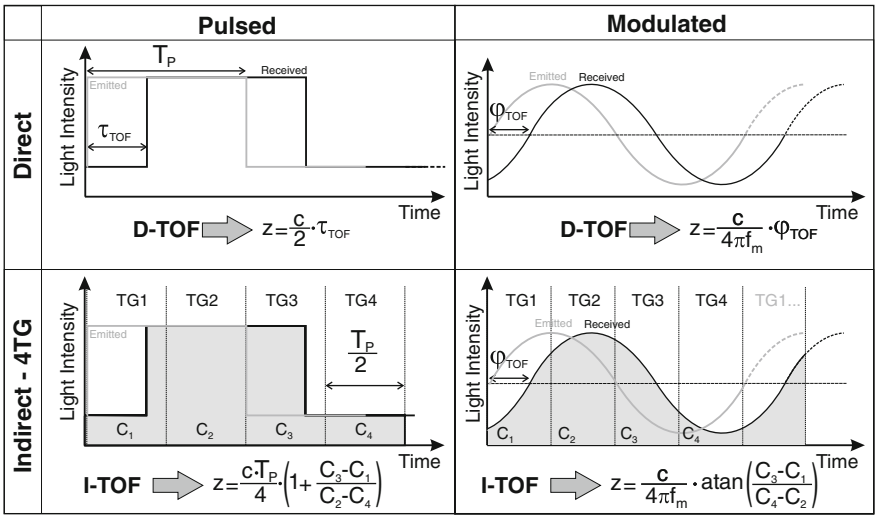

Fig. 2 Overview of pulsed and modulated D-TOF and I-TOF measuring techniques

full-custom detectors have been developed for this class of systems. They can be mainly classified in three categories:

(a) *In-Pixel Photo-mixing Devices*. This approach exploits photo-demodulators, in which the photo-generated charge is mixed toward two or more collection electrodes thus achieving an intrinsic photo-mixing effect.
(b) *Standard photodiodes coupled to dedicated processing circuitry*. This approach exploits the extensive use of switched-capacitors electronics (either in the pixel or at the periphery) to recover the distance information from the current photo-generated by the photodiode.
(c) *Single-Photon Avalanche Diodes (SPADs) coupled to proper processing circuitry*. With respect to (b), an avalanche diode, operating in Geiger regime to achieve sensitivity to individual photons, is used to collect the light echo and coupled to a readout and processing electronics aimed at extracting the Time-Of-Flight information.

The most mature solution is represented by sensors belonging to a), and most of the 3D cameras available on the market are actually based on this concept [24–39]. The main advantage of this approach is the read-out channel simplicity, which results in a small pixel size; the main problems are the sensitivity to the ambient light and the cost of non-standard technologies (e.g. CCD/CMOS, customized CMOS, high resistivity substrate, etc.), that are often required.

The use of complex in-pixel electronics, used to properly process and accumulate the photo-generated charge, makes sensors belonging to b) being characterized by large pixel pitch and relatively high power consumption [40–48]. Moreover, they typically exhibit lower precision with respect to (a) and (c)

because of the noise contribution introduced by the numerous transistors introduced in the signal path. On the other hand, ad hoc processing structures can be implemented at pixel- or column-level to successfully remove most of the common mode signal, thus implementing background resilient sensors that can be used for outdoor operation such as automotive and security.

Finally, sensors based on category (c) have been widely used in high-performance single-point scanner systems since the 80s, using avalanche photodiodes (APDs) fabricated within dedicated technologies coupled to discrete-components read out and processing electronics or measurement instruments. However, only recently, the possibility of implementing good performance APDs/SPADs in CMOS technologies opened the way to the realization of range image sensors based on this approach [12–23, 49–51].

The great advantage of this solution is the extremely high sensitivity of the photodetector, capable of detecting down to single-photon, and the intrinsic low-noise performance that allows operating at the shot-noise limit.

The above mentioned sensor categories will be extensively described in Chaps. 2, 3 and 4 where the state-of-the-art for each approach will be analyzed through circuital and device implementations peculiar of each sensor architecture.

4 Conclusions

Image sensors capable of detecting arrival times of impinging light signals with sub-nanosecond time resolution are becoming more and more important in many applications. Among them, TOF 3D cameras represent one of the markets having the largest possibilities of expansion thanks to the numerous sectors of exploitation of such a technology. The extra information provided by 3D cameras, with respect to standard 2D imagers, is fundamental to acquire a reliable model of the scene under measurement, opening the way to new detection paradigms in the field of machine vision. Industrial control, next generation user interfaces based on gesture recognition, advanced vision systems for automotive, etc. are just a few examples of important sectors using 3D-imaging technology.

In this chapter the operation principle of TOF cameras has been described and the main TOF sensor architectures presented so far have been reviewed. This is mainly an introduction to extended descriptions provided in Chaps. 2, 3 and 4 that will deal with TOF sensors based on SPAD, electronic shutter and photo-mixing devices respectively.

Regardless of the numerous solutions proposed in the scientific literature in the last few years and although several commercial products are now available in the field of TOF 3D cameras, there are still several aspects that can be improved. Ambient light immunity and dynamic range enhancement are two key features for the next generation of 3D cameras, while as in conventional cameras, there is a continuous demand of higher resolution and frame rate, as well as reduced power

consumption. The addition of color in the same sensor is also a very appealing feature, and the first attempts to implement this functionality are being carried out.

The development of TOF technology should also take into account competing technologies, such as those based on pattern projection and stereo imaging. Those systems successfully demonstrated that accessing consumer market could dramatically reduce the system cost. In fact, the building blocks of system like [11] are quite similar to the ones needed by TOF cameras, i.e. illuminator, custom image sensor, and optics, however, the final cost of this system is one order of magnitude lower than the cost of TOF camera products.

The main drawbacks of systems based on pattern projection and stereo image matching with respect to TOF technology are: (i) the limited scalability of the system size due to the need of a baseline (ii) the high computational effort required to extract the depth information that limits the sensor frame rate and the minimum power consumption, and finally (iii) the generation of artifacts under some measurement conditions.

The next three to five years will demonstrate all the potential of TOF technology and will reveal if the evolution of TOF cameras will follow the same amazing expansion experienced by conventional CMOS cameras in the 2000s.

References

1. R. Schwarte, Principles of 3-D Imaging Technology, in *Handbook of Computer Vision and Applications*, ed. by B. Jähne, H. Haussecker, P. Geißler (Academic Press, 1999)
2. B. Jähne, H. Haussecker, P. Geißler, *Handbook of Computer Vision and Applications*, vol. 1 (Academic Press, San Diego, 1999) pp. 479–482
3. P. Besl, Active optical range imaging sensors. Mach. Vis. Appl. **1**, 127–152 (1988)
4. E.M. Mikhail, J.S. Betherl, J.C. McGlone, *Introduction to modern photogrammetry* (John Wiley & Sons, Inc., New York, 2001)
5. M.-C. Amann, T.B.M. Lescure, R. Myllyla, M. Rioux, Laser ranging: a critical review of usual techniques for distance measurement. Opt. Eng. **40**, 10–19 (2001)
6. F. Blais, Review of 20 years of range sensor development. J. Elect. Imaging **13**(1), 231–243 (2004)
7. B. Hosticka, P. Seitz, A. Simoni, Optical Time-Of-Fight sensors for solid-state 3D-vision. Encycl. Sens. **7**, 259–289 (2006)
8. Leica-geosystem website, www.leica-geosystems.com
9. Konicaminolta website, www.konicaminolta.com
10. F. Menna, F. Remondino, R. Battisti, E. Nocerino, Geometric investigation of a gaming active device. Proc. SPIE Opt. Metrol. **8085**(1), 80850G (2011)
11. K. Khoshelham, sO Elberink, Accuracy and resolution of kinetic depth data for indoor mapping applications. Sensors **12**, 1437–1454 (2012). doi:10.3390/s120201437
12. M.A. Albota et al. Three-dimensional imaging laser radars with geiger-mode avalanche photodiode arrays. Lincoln Labs J. **13**(2) 351–370 (2002)
13. C. Niclass, A. Rochas, P.A. Besse, E. Charbon, Design and characterization of a CMOS 3-D image sensor based on single photon avalanche diodes. IEEE J. Solid-State Circuits **40**(9), 1847–1854 (2005)

14. J. Richardson, R. Walker, L. Grant, D. Stoppa, F. Borghetti, E. Charbon, M. Gersbach, R. K. Henderson, A 32 × 32 50 ps resolution 10 bit time to digital converter array in 130 nm CMOS for time correlated imaging, in *IEEE Custom Integrated Circuits Conference* (2009) pp. 77–80
15. M. Gersbach, Y. Maruyama, E. Labonne, J. Richardson, R. Walker, L. Grant, R. K. Henderson, F. Borghetti, D. Stoppa, E. Charbon, "A Parallel 32 × 32 time-to-digital converter array fabricated in a 130 nm imaging CMOS technology", in *IEEE European Solid-State Device Conference* (2009)
16. C. Veerappan, J. Richardson, R. Walker, D.U. Li, M.W. Fishburn, Y. Maruyama, D. Stoppa, F. Borghetti, M. Gersbach, R.K. Henderson, E. Charbon, A 160 × 128 single-photon image sensor with on-pixel, 55 ps 10b time-to-digital converter, in *IEEE International Solid-State Circuits Conference* (2011) pp. 312-314
17. D. Stoppa, F. Borghetti, J. Richardson, R. Walker, L. Grant, R.K. Henderson, M. Gersbach, E. Charbon, "A 32 × 32-pixel array with in-pixel photon counting and arrival time measurement in the analog domain, in *IEEE European Solid-State Device Conference* (2009) pp. 204–207
18. R. J. Walker, J. R. Richardson, R. K. Henderson; A 128 × 96 pixel event-driven phase-domain ΔΣ-based fully digital 3D camera in 0.13 μm CMOS imaging technology, *IEEE International Solid-State Circuits Conference* (2011) pp. 410–412
19. M. A. Itzler, M. Entwistle, M. Owens, K. Patel, X. Jiang, K. Slomkowski, S. Rangwala, Geiger-mode avalanche photodiode focal plane arrays for three-dimensional imaging LADAR. SPIE Infrared Remote Sens. Instrum. 7808 (2010)
20. B Aull, J. Burns, C. Chenson, B. Felton, H. Hanson, C. Keast, J. Knecht, A. Loomis, M. Renzi, A. Soares, S. Vyshnavi, K. Warner, D. Wolfson, D. Yost, D. Young, Laser radar imager based on 3D integration of geiger-mode avalanche photodiodes with two SOI timing circuit layers. IEEE Int. Solid-State Circuits Proc. 304–305 (2006)
21. C. Niclass, C. Favi, T. Kluter, F. Monnier, E. Charbon, Single-photon synchronous detection. IEEE J. Solid-State Circuits **44**(7), 1977–1989 (2009)
22. C. Niclass, M. Soga, S. Kato, A 0.18 μm CMOS single-photon sensor for coaxial laser rangefinders, in *Asian Solid-State Circuits Conference* (2010)
23. L. Pancheri, N. Massari, F. Borghetti, D. Stoppa, A 32 × 32 SPAD pixel array with nanosecond gating and analog readout, *International Image Sensor Workshop* (*IISW*), Hokkaido 8–11 June 2011
24. Mesa Imaging website, www.mesa-imaging.ch
25. PMD Technologies website, www.pmdtec.com
26. SoftKinetic website, www.softkinetic.com
27. T. Spirig, P. Seitz, O. Vietze, F. Heitger, The lock-in CCD two dimensional synchronous detection of light. IEEE J. Quantum Electron. **31**, 1705–1708 (1995)
28. R. Miyagawa, T. Kanade, CCD-based range-finding sensor. IEEE Trans. Electron Dev. **44**(10), 1648–1652 (1997)
29. S. Kawahito, I.A. Halin, T. Ushinaga, T. Sawada, M. Homma, Y. Maeda, A CMOS Time-Of-Flight range image sensor with gates-on-field-oxide structure. IEEE Sens. J. **7**(12), 1578–1586 (2007)
30. D. Van Nieuwenhove, W. Van Der Tempel, M. Kuijk, Novel standard CMOS detector using majority current for guiding photo-generated electrons towards detecting junctions, in *Proceedings of IEEE/LEOS Symposium, Benelux Chapter*, pp. 229–232 (2005)
31. W. van der Tempel, R. Grootjans, D. Van Nieuwenhove, M. Kuijk, A 1k-pixel 3-D CMOS sensor, in *Proceedings of IEEE Sensors Conference* (2008) pp. 1000–1003
32. G.-F. Dalla Betta, S. Donati, Q.D. Hossain, G. Martini, L. Pancheri, D. Saguatti, D. Stoppa, G. Verzellesi, Design and characterization of current-assisted photonic demodulators in 0.18-μm CMOS technology. IEEE Trans. Electron Dev. **58**(6), 1702–1709 (2011)
33. L. Pancheri, D. Stoppa, N. Massari, M. Malfatti, L. Gonzo, Q. D. Hossain, G.-F. Dalla Betta, A 120x160 pixel CMOS range image sensor based on current assisted photonic

demodulators. in *Proceedings of SPIE*, vol. 7726 (SPIE Photonics Europe, Brussels, Belgium, 2010) pp. 772615
34. D. Stoppa, N. Massari, L. Pancheri, M. Malfatti, M. Perenzoni, L. Gonzo, A range image sensor based on 10-μm lock-in pixels in 0.18-μm CMOS imaging technology. IEEE J. Solid-State Circuits **46**(1), 248–258 (2011)
35. H.-J. Yoon, S. Itoh, S. Kawahito, A CMOS image sensor with in-pixel two-stage charge transfer for fluorescence lifetime imaging. IEEE Trans. Electron Dev. **56**(2), 214–221 (2009)
36. L.-E. Bonjour, T. Baechler, M. Kayal, High-speed general purpose demodulation pixels based on buried photodiodes, in *Proceedings of IISW* 2011 (Hokkaido, June 8–11, 2011)
37. C. Tubert, L. Simony, F. Roy, A. Tournier, L. Pinzelli, P. Magnan, High speed dual port pinned-photodiode for Time-Of-Flight imaging, in *Proceedings of IISW 2009* (Bergen, Norway, June 26–28, 2009)
38. H. Takeshita, T. Sawada, T. Iida, K. Yasutomi, S. Kawahito, High-speed charge transfer pinned-photodiode for a CMOS Time-Of-Flight range image sensor. Proc. SPIE **7536**, 75360R (2010)
39. S.-J. Kim, J.D.K. Kim, S.-W. Han, B. Kang, K. Lee, C.-Y. Kim "A 640 × 480 image sensor with unified pixel architecture for 2D/3D imaging in 0.11 μm CMOS. IEEE Symp VLSI Circuits, 92–93 (2011)
40. R. Jeremias, W. Brockherde, G. Doemens, B. Hosticka, L. Listl, P. Mengel, A CMOS photosensor array for 3D imaging using pulsed laser. IEEE Int. Solid-State Circuits Conf. 252–253 (2001)
41. D. Stoppa, L. Viarani, A. Simoni, L. Gonzo, M. Malfatti and G. Pedretti, "A 50 × 30-pixel CMOS sensor for TOF-based Real Time 3D Imaging", *Workshop on Charge-Coupled Devices and Advanced Image Sensors*, Karuizawa, Nagano, 2005
42. M. Perenzoni, N. Massari, D. Stoppa, L. Pancheri, M. Malfatti, L. Gonzo, A 160 × 120-pixels range camera with in-pixel correlated double sampling and fixed-pattern noise correction. IEEE J. Solid-State Circuits **46**(7), 1672–1681 (2011)
43. O. Sgrott, D. Mosconi, M. Perenzoni, G. Pedretti, L. Gonzo, D. Stoppa, A 134-pixel CMOS sensor for combined Time-Of-Flight and optical triangulation 3-D imaging. IEEE J. Solid-State Circuits **45**(7), 1354–1364 (2010)
44. K. Oberhauser, G. Zach, H. Zimmermann, Active bridge-correlator circuit with integrated PIN photodiode for optical distance measurement applications, in *Proceedings of the 5th IASTED International Conference Circuits, Signals and Systems* (July 2007) pp. 209–214
45. G. Zach, A. Nemecek, H. Zimmermann, Smart distance measurement line sensor with background light suppression and on-chip phase generation, in *Proceedings of SPIE, Conference on Infrared Systems and Photoelectronic Technology III*, vol. 7055 (Aug 2008) pp. 70550P1–70550P10
46. G. Zach, H. Zimmermann, A 2 × 32 range-finding sensor array wit pixel-inherent suppression of ambient light up to 120klx, in *IEEE International Solid-State Circuits Conference* (2009) pp. 352–353
47. G. Zach, M. Davidovic, H. Zimmermann, A 16 × 16 pixel distance sensor with in-pixel circuitry that tolerates 150 klx of ambient light. IEEE J. Solid-State Circuits **45**(7), 1345–1353 (2010)
48. C. Niclass, C. Favi, T. Kluter, M. Gersbach, E. Charbon, A 128 × 128 single-photon image sensor with column-level 10-bit time-to-digital converter array. IEEE J. Solid-State Circuits **43**(12), 2977–2989 (2008)
49. C. Niclass, M. Sergio, E. Charbon, A CMOS 64x48 single photon avalanche diode array with event-driven readout, in *IEEE European Solid-State Circuit Conference* (2006)
50. J.S. Massa, G.S. Buller, A.C. Walker, S. Cova, M. Umasuthan, A.M. Wallace, Time-pf-flight optical ranging system based on time-correlated single-photon counting. App. Opt. **37**(31), 7298–7304 (1998)
51. D. Stoppa, L. Pancheri, M. Scandiuzzo, L. Gonzo, G.-F. Della Betta, A. Simoni, A CMOS 3-D imager based on single photon avalanche diode. IEEE Trans. Circuits Syst. **54**(1), 4–12 (2007)

SPAD-Based Sensors

Edoardo Charbon, Matt Fishburn, Richard Walker, Robert K. Henderson and Cristiano Niclass

1 Introduction

3D imaging and multi-pixel rangefinding constitute one of the most important and innovative fields of research in image sensor science and engineering in the past years. In rangefinding, one computes the Time-Of-Flight of a ray of light, generated by a mono-chromatic or wide-spectral source, from the source through the reflection of a target object and to a detector. There exist at least two techniques to measure the Time-Of-Flight (TOF): a direct and an indirect technique. In direct techniques (D-TOF), the time difference between a START pulse, synchronized with the light source, and a STOP signal generated by the detector is evaluated. In indirect techniques (I-TOF), a continuous sinusoidal light wave is emitted and the phase difference between outgoing and incoming signals is measured. From the phase difference, the time difference is derived using well-known formulae.

Single-photon avalanche diodes (SPADs) or Geiger-mode avalanche photodiodes (GAPDs) are detectors capable of capturing individual photons with very high time-of-arrival resolution, of the order of a few tens of picoseconds. They

E. Charbon (✉) · M. Fishburn
TU Delft, Mekelweg 4 2628CD Delft, The Netherlands
e-mail: e.charbon@tudelft.nl

M. Fishburn
e-mail: m.w.fishburn@tudelft.nl

R. Walker · R. K. Henderson
The University of Edinburgh, Faraday Bldg., King's Buildings
EH9 3JL Edinburgh, Scotland, U.K
e-mail: richard.walker@ed.ac.uk

R. K. Henderson
e-mail: robert.henderson@ed.ac.uk

C. Niclass
EPFL, 1015 Lausanne, Switzerland
e-mail: cristiano.niclass@epfl.ch

F. Remondino and D. Stoppa (eds.), *TOF Range-Imaging Cameras*,
DOI: 10.1007/978-3-642-27523-4_2,

may be fabricated in dedicated silicon processes or in standard CMOS technologies. Most SPADs generally operate at room temperature, but they may also be cooled for better noise performance. Even though solid-state SPADs implemented in III–V materials exist, and the literature on the subject is extensive, in this chapter, we limit our attention to silicon devices.

Cova and McIntyre started advocating the use of SPADs for fast timing applications in the 1980s [1, 2]. Thanks to their picosecond timing resolution, SPADs are a natural candidate for D-TOF techniques. If one wants a distance resolution of, say, 1 mm, one needs to discriminate light pulses with a resolution of 6.6 ps (a round-trip Time-Of-Flight is assumed). However, such a time uncertainty is not achievable with a room temperature SPAD implemented in any silicon technology. Thus, averaging and multi-measurement techniques must be employed. A common choice is the use of time-correlated single-photon counting (TCSPC). The technique assumes that a START or synchronization signal is always present at the beginning of each measurement cycle, while the STOP signal is provided by the detector, in our case a SPAD, at a much smaller frequency, typically 10^4–10^6 smaller than that of the synchronization. If this condition is satisfied—and it is often required to minimize pile-up effects—several thousands of time-of-arrival evaluations are needed for each frame to achieve an accurate Time-Of-Flight measurement. A reverse START-STOP arrangement is also possible, depending upon the architecture of the imager, whereas a higher jitter of the measurement system might incur if high intra-optical-pulses jitter is present in the light source.

SPADs may also be used in I-TOF mode of operation. In this chapter two complementary techniques are presented. The common principle is that of quickly switching the SPAD to divert its output signal appropriately, depending on the time-of-arrival. Indirect detection techniques may also be handled in a completely digital environment, thus simplifying the electronics and control signals and enabling large arrays of pixels to be implemented in standard CMOS technologies.

The chapter is organized as follows. After an introduction to the physical mechanisms underlying SPADs, an overview of SPAD fabrication techniques is given, followed by a detailed description of direct and indirect techniques for Time-Of-Flight measurement; the description is complemented by examples of SPAD array implementations in CMOS and relative characterization. An outlook concludes the chapter.

2 The Physics of SPADs

An avalanche photodiode (APD) is a p-n junction that relies on impact ionization effects to multiply photon-generated electrons and holes. APDs output a pulse of electric current synchronous, with some time uncertainty, to the arrival of a single photon. In APD-based, Time-Of-Flight detectors and image sensors, external circuitry senses and analyzes this current pulse to find the photon's time-of-arrival, thus inferring the range; this process, known as rangefinding, enables the reconstruction

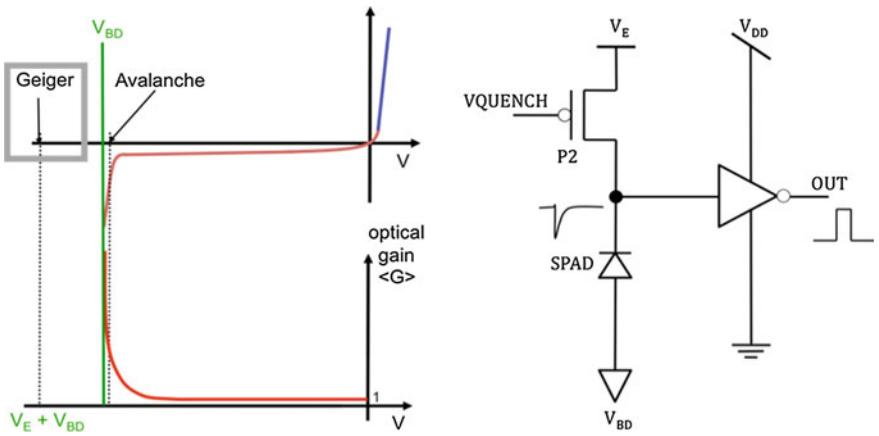

Fig. 1 Steady-state I–V characteristics for a p-n junction with Geiger and avalanche mode of operation (*left*). Passively quenched SPAD (*right*). V_E is known as the excess bias voltage at which a diode must be biased in Geiger mode; it represents the voltage in excess of or above the breakdown voltage V_{BD}. A comparator or inverter is used to shape the output pulse of the detector

of 3D scenes non-destructively. This section gives an overview of the fundamental mechanisms governing the avalanche pulse, focusing on the factors that contribute to the time uncertainty and ultimately the distance estimation accuracy.

Generally, when electrical engineers think of the I–V characteristics of a p-n junction, they think of the steady state curve, shown in Fig. 1. However, there is a pseudo-steady-state in the breakdown operating condition—a voltage above[1] the breakdown voltage can be applied so long as no carriers exist in the diode's depletion region. As soon as a carrier is injected into the depletion region, impact ionization may cause an avalanche to occur, and the diode will shift operating points to the steady-state curve. Impact ionization's underlying statistical process, which is dependent on the electric field, material, and ambient conditions, governs the probability that an avalanche will occur. If the electric field magnitude is high enough, then both electrons and holes are expected to cause significant ionization, the avalanche will become self-sustaining, and the avalanche photodiode is operating in Geiger mode.[2]

If the field magnitude is only sufficient for electrons to cause significant ionization but not holes, the APD is in linear mode. Quantitatively a diode is in Geiger mode when it meets the condition

$$1 \leq \int_0^W \alpha \cdot \exp\left(\int_x^W (\beta - \alpha)\mathrm{d}x'\right) \mathrm{d}x, \tag{1}$$

[1] The preposition "above" is used because researchers working with APDs consider the cathode to be the terminal with the higher voltage.

[2] Termed after the similarity to a Geiger counter.

with α and β representing the impact ionization rates (per m) of electrons and holes, respectively, and W is the depletion width. The bias at which Eq. (1) is an equality is called the breakdown voltage, V_{BD}. The bias applied to the diode, V_{OP}, exceeds breakdown by a voltage known as excess bias voltage, V_E. Henceforth the discussion will be restricted to SPAD technologies [3].

A SPAD is able to detect more than a single carrier by the inclusion of external circuitry, which quenches an avalanche by: sensing an avalanche; lowering the voltage applied to the SPAD; and after some time, raising the applied voltage above the breakdown voltage. The simplest such circuit is a resistor placed in series with the diode, also known as ballast resistor. The circuit works as follows. First, when there are no free carriers in the junction, the applied voltage on the diode is V_{OP}. When light injects a carrier into the junction, impact ionization may or may not cause the rapid build-up of free carriers in a small part of the diode. If significant ionization does not occur and all free carriers are swept out of the depletion region, the incident photon is not detected. If ionization does occur, it will continue until the space-charge phenomena limits the local carrier concentration. The avalanche will spread to other regions of the diode via a multiplication-assisted diffusion process. The decrease in voltage across the diode, dependent on both any parasitic capacitances and the quenching resistor, will eventually reach the excess bias. At this point the diode is quenched—no further current should flow from impact ionization and there are no free carriers in the diode itself. The voltage will then be recharged by the flow of electric current through the quenching resistor into the parasitic capacitances, with the diode being ready to detect another carrier after this dead time [4].

The probability that a single photon's generated carriers are detected is called the photon detection probability (PDP). A number of factors influence the PDP, including electric field conditions, doping levels, whether electrons or holes primarily initiate avalanches, and the applied voltage. Photons are not the only source of initial carriers; uncorrelated or correlated noise can also cause free carrier injection and undesirable avalanches. Uncorrelated noise sources include: ambient light; tunneling from an electric field that is too high; and fabrication defects which ease valence-to-conduction band transitions, such as thermally generated or tunneling carriers. The last factor, fabrication defects, can also cause afterpulsing, a type of time-correlated noise. Traps in the forbidden energy band can fill, only to release free carriers on the time scale of tens of nanoseconds following an avalanche. Afterpulsing prevents an instant recharge phase in SPADs, and places constraints on the minimum dead time.

There are other sources of correlated noise besides afterpulsing—optical and electrical crosstalk are the most common, but in practice afterpulsing is the dominant type of correlated noise. Whether the initial carrier is photon-generated or not, several factors cause time uncertainty between the injection time and the sense time. The most important timing factor is whether the carrier is generated in the depletion region itself, or if it must diffuse into the depletion region. Carriers that successfully diffuse into the depletion region do so following an exponential

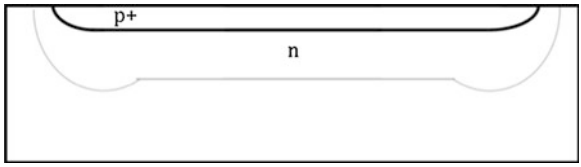

Fig. 2 Cross-sections of a generic pn junction in a planar process with the depletion region (*gray line*) forming in the structure upon reverse-biasing, assuming a large doping differential between the p and n regions

time distribution [5]. Once the initial carrier is in the depletion region, the statistics of impact ionization will create a time uncertainty that is roughly a normal distribution. The overall timing response of a SPAD to a pulsed laser can be described as a background noise plus a normal distribution convolved with the addition of an impulse function (describing carriers generated in the depletion region) with an exponential distribution.

3 CMOS SPAD Design

Building SPADs in CMOS substrates requires knowledge of the process and layers available to the designer to implement junctions that can be reverse-biased at high voltages. Figure 2 shows a generic pn junction implemented in a planar process. The figure shows the depletion region, as it forms upon reverse biasing the junction (assuming a large doping differential between the p and n regions).

Implementing a pn junction in a planar process first involves finding a way to prevent premature edge breakdown (PEB). Several techniques exist to implement PEB prevention. In essence, the techniques have in common the reduction of the electric field or the increase of the breakdown voltage at the edges of the junction, so as to maximize the probability that the avalanche is initiated in the center of the multiplication region, i.e. the region where the critical electric field for impact ionization is reached and, possibly, exceeded.

Figure 3 illustrates four of the most used structures. In (a) the n+ layer maximizes the electric field in the middle of the diode. In (b) the lightly doped p- implant reduces the electric field at the edge of the p+ implant. In (c) a floating p implant locally increases the breakdown voltage. A polysilicon gate is usually drawn to prevent the creation of a shallow trench, however, it can also be used to further extend the depletion region.

Shallow trench isolation (STI) can also be used to delimit the junction, provided that it is surrounded by a multi-layer of doped silicon so as to force recombination of those charges generated in the defect-rich STI as shown in structure (d) [6]. These structures are usually shaped as a ring around the junction; they are known as *guard rings*. Guard rings can also be defined *implicitly* by proper definition of drawn layers [7].

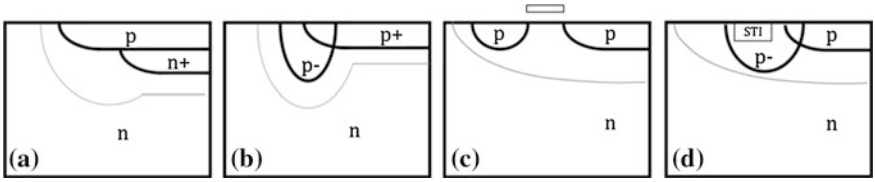

Fig. 3 Cross-sections of doping profiles that may be used to prevent premature edge breakdown in planar processes

There exist a variety of avalanche quenching techniques, partitioned in active and passive methods. The literature on these variants is extensive [8]. In active methods, the avalanche is detected and stopped by acting on the bias. In passive methods the pn junction bias is self-adjusted e.g. by a ballast resistor. Recharge methods can also be active and passive. In active methods, the bias across the diode is re-established by a switch activated by an avalanche detector. In passive methods the recharge occurs through the ballast.

Upon photon detection, the device generates a current pulse that is converted to a digital voltage level by means of a pulse shaping circuitry, also shown in the figure. The pulse shaper is also acting as an impedance adapter to drive the load of the column readout often employed in a SPAD matrix.

The main parameters characterizing individual SPADs are sensitivity, measured as **photon detection probability** (PDP), noise, measured as the rate of spurious pulses due to thermal events or **dark count rate** (DCR). Other parameters include **timing jitter**, also known somewhat inappropriately as **timing resolution**, **afterpulsing probability** and the aforementioned **dead time**. These parameters have been used in the literature for a variety of CMOS processes [9–17].

When implemented in an array, other performance measures become relevant to the quality of the imager. Dead time uniformity relates to the variability in dead time, which determines the dynamic range of each detector. Timing jitter uniformity and PDP uniformity, as well as DCR uniformity and crosstalk have to be accounted for and properly characterized [9]. PDP of course will also be a function of the input wavelength. In CMOS SPAD implementations, the sensitivity range is mostly in the visible spectrum, with a somewhat reduced near infrared and near ultraviolet PDP.

Crosstalk is also a chip-level effect similar to PDP and DCR non-uniformities; it relates to the interaction between an aggressor pixel and a victim pixel, where the aggressor may cause a spurious avalanche in a victim. The effect can be electrical and/or optical. Electrical crosstalk is due to electrical interference through substrate or supply noise. Optical crosstalk may occur when an avalanche is triggered in the aggressor; by impact ionization, several photons may be emitted, thus causing the victim to detect them. While electrical crosstalk is strongly dependent on the design of supply lines and of substrate noise rejection measures, optical crosstalk may only be influenced by the number of carriers involved in an avalanche and by pixel pitch.

4 TCSPC Based TOF Camera Systems

Using TCSPC for optical rangefinding in D-TOF mode has been proposed several decades ago, since the introduction of the LIDAR concepts. SPAD based single-pixel detectors, in combination with scanning, powerful pulsed light sources. One of the first examples of this combination was proposed in [18, 19]. In this work, the light source is synchronized to the SPAD to produce an accurate evaluation of the Time-Of-Flight of the reflected photons and thereby of the distance to the target.

In [20] this concept was made scannerless thanks to the use of monolithic arrays of SPADs implemented in CMOS technology. The concept, described in Fig. 4, is enabled by the use of a cone of light reaching approximately simultaneously the target source.

The photons reflected by the surface are imaged through a lens system to the array. With the use of an accurate chronometer or stop watch, it is possible to derive the distance of the reflecting point using the following relation

$$d \cong \frac{c}{2} \cdot \tau_{TOF}, \tag{2}$$

where τ_{TOF} is the Time-Of-Flight or the time difference between the light pulse synchronization signal and the time-of-arrival in the detector, and c is the speed of light in vacuum. Since SPADs are dynamic devices, they generate a digital pulse upon detection of a photon, and thus, unlike conventional diodes, they cannot hold a charge proportional to the overall photon count. Thus, the Time-Of-Flight must be computed in situ (either on pixel, on column, or on chip) or outside the image sensor. The same holds with integrated time-of-arrival evaluation: it can only be (1) in-pixel, (2) in-column, or (3) on-chip. To address this limitation, researchers have adopted a number of architectures that take advantage of the low propagation delay or high level of miniaturization achievable in standard submicron and deep-submicron CMOS technologies.

The simplest readout architecture implementing photon counting on-chip in combination with random-access single-photon detection, was demonstrated for the first time in a matrix of 32 × 32 pixels, each with an independent SPAD, a

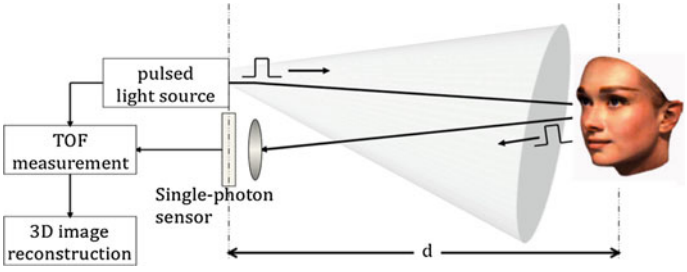

Fig. 4 Time-correlated single-photon counting (TCSPC) for optical rangefinding and 3D imaging

quenching mechanism, a pulse shaping and column access circuitry [20]. In this readout scheme, all time-sensitive operations had to be performed sequentially. This design has the main drawback in that it can only "see" one pixel at any point in time, while all the other pixels are operating but their output is lost. The micrograph of the chip is shown in Fig. 5; the chip was implemented in a 0.8 μm high-voltage CMOS process.

Addressing the readout bottleneck required some degree of sharing. The column is the obvious place to start from, since it is a repetitive structure that touches all pixel rows. The first known such approach involved interpreting the column as a bus. The bus is used as transfer time and address over the same hardware. The time is coded in partially processed pulses generated in the pixel of which the time-of-arrival is evaluated. The address is coded as a unique combination over the lines present in the bus sent to the bottom of the column where the time-of-arrival is evaluated, either off or on chip [11].

The second approach, known as latchless pipelined readout, has a passive type of coding, whereas time-of-arrival also contain the information of the row position where the pulse was generated. Every photon triggers a pulse that is injected onto the pipeline at a precise location that corresponds to the physical place where the pixel is located. Since the propagation time is across the column is too short to enable any time-based discrimination, a timing-preserving delay line is added to the column. At the bottom of the column time discrimination is performed by a column-based TDC that also returns the row code [21]. The photomicrograph

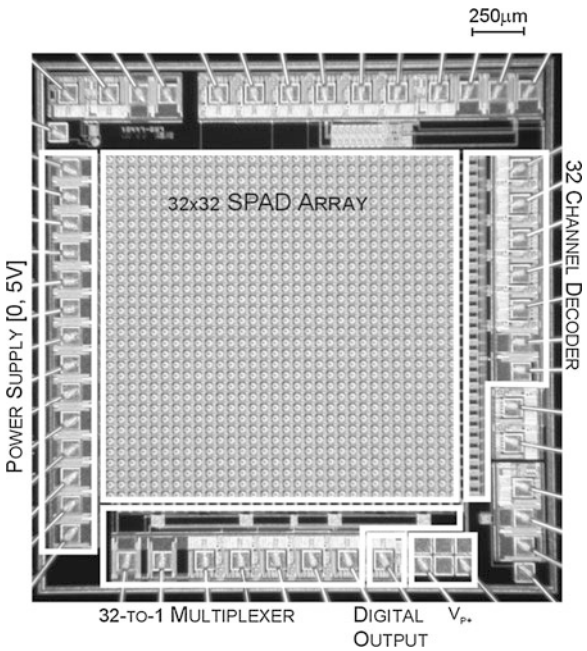

Fig. 5 The first large SPAD array with random access readout. The chip was implemented in 0.8 μm CMOS technology

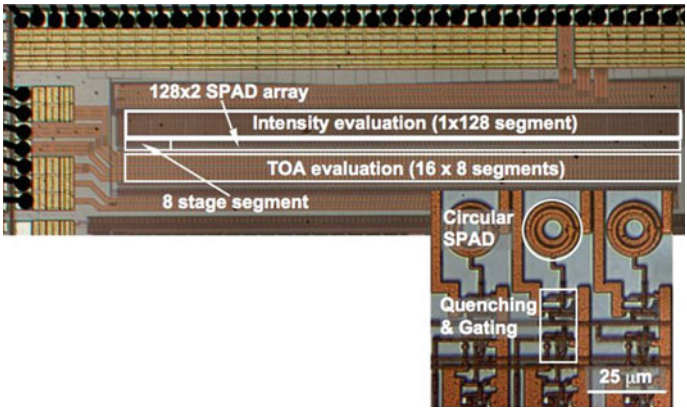

Fig. 6 CMOS version of a latchless pipeline based readout fabricated in 0.35 µm CMOS technology [21]

shown in Fig. 6 illustrates the actual implementation of the concept for a latchless pipelined 128 × 2 SPAD array fabricated in 0.35 µm CMOS.

An important step towards full parallelism was achieved with LASP [10], a 128 × 128 SPAD array, where a bank of 32 column-parallel time-to-digital converters (TDCs) was used to simultaneously process 128 in-line SPADs using an event-driven 4-to-1 column-multiplexer (one per column). Figure 7 shows the block diagram of LASP. Each TDC in the 32-array can generate 10 MS/s with a time resolution of 97 ps. The resolution can be further increased to 70 ps by acting on the clock frequency. Each TDC in LASP is a 3-tier partial TDC based on three different architectures: a clocked counter (2 MSBs, 25 ns resolution), a phase

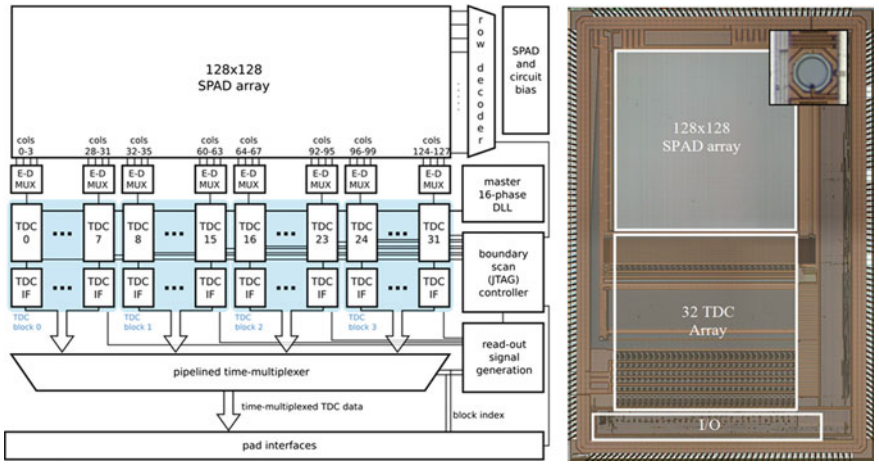

Fig. 7 Schematic and micrograph of LASP; an array of 32 TDCs processes the pulses generated by 128 SPADs at any time by means of a 4-to-1 event-driven multiplexer (one for each TDC)

interpolator controlled by a temperature-compensated DLL (4 intermediate bits, 1.56 ns resolution), and a 16-taps Vernier line (4 LSBs, 97.6 ps resolution). The total time resolution of 10bits is routed outside the chip through a high-speed digital network operating at 3.2 Gb/s. The differential non-linearity (DNL) and integral non-linearity (INL) were recently improved to ±0.1LSB and ±0.25LSB, respectively [22].

The chip was tested in TCSPC mode to compute a scene's depth via a pixel-by-pixel Time-Of-Flight evaluation of a defocused beam hitting the target. The results of the experiment are shown in the histogram of Fig. 8. The jitter is dominated by the SPAD timing uncertainty, whereas the characteristic tail of the device also appears from the picture.

The distance evaluation result is shown in Fig. 9 as a function of the real distance measured using a precision device from 40 cm to 3.75 m. Each distance measurement was derived from the centroid of the corresponding histogram, whereas the uncertainty as a function of distance is plotted in also plotted in the figure.

In Fig. 10 the resulting 3D image of a mannequin illuminated by a cone of pulsed laser light with a wavelength of 637 nm is shown after a 1 s exposure. The 3D points represent the centroid of the histograms of each pixel.

The integration of time-resolving electronics on a per-column or per-chip basis represents a trade-off between fill-factor, processing bandwidth and circuit area. Unlike integrating image sensors based on photodiodes, photons falling on SPAD pixels which are not multiplexed to available time-resolving channels are lost. In an efficient SPAD sensor operating in D-TOF mode, a time-stamp must be generated for every impinging photon at every pixel detector. This necessitates the combination of per-pixel time-digitization circuitry and high speed array readout.

The integration of a large array of in-pixel TDCs or time-to-amplitude converters (TACs) poses several challenges with respect to single channel architectures found in the literature [23–26]:

1. Circuit area is limited to a few 100 μm^2 to achieve practical pixel fill-factor and pitch.
2. Power consumption cannot exceed a few 100 μA per pixel, in order to allow array size to be scaled to 10's of kilopixels without excessive heating.

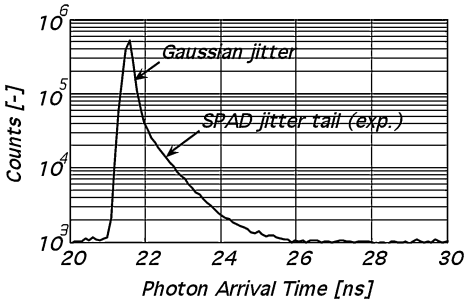

Fig. 8 TCSPC experiment. The laser pulse is pointed toward a SPAD in the array and the time-of-arrival of the first detected photon is evaluated by the corresponding TDC. The resulting histogram, shown in the plot in logarithmic scale, is then computed [10]

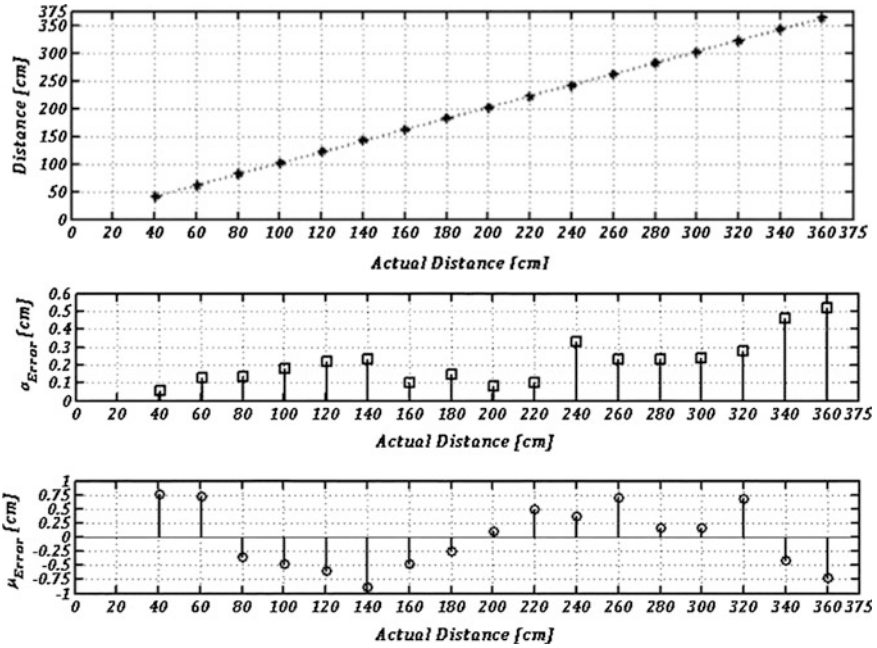

Fig. 9 Actual distance versus estimated distance computed in LASP at room temperature (*top*); average error versus distance (*middle*); standard deviation versus distance (*bottom*) [10]

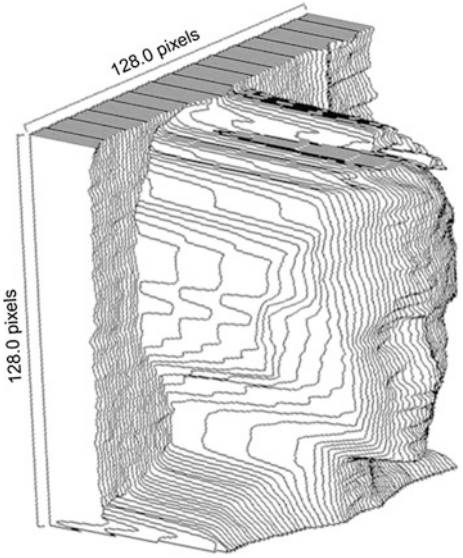

Fig. 10 Target image computed by LASP in 1 s exposure at room temperature [10]